NASA-CR-202249



*A Annual Report to the National Aeronautics and Space Administration in Dynamics of the Solid Earth Program*

for the period of March 1, 1995 - September 1, 1996

NASA GRANT NAG5-1905

# Strategies for Space-Geodetic Monitoring of Infraseismic and Subseismic Transient Deformations

PRINCIPAL INVESTIGATOR:

Thomas H. Jordan
Shrock Professor of Earth and Planetary Science
Department of Earth, Atmospheric, and Planetary Sciences
MIT, Room 54-918
Cambridge, MA 02139
(617)-253-3382, thj@mit.edu

# Annual Technical Report, 3/1/95 to 9/1/96
# NASA GRANT NAG5-1905
# T. H. Jordan, Principal Investigator

Infraseismic and subseismic deformation transients have been observed by seismic and geodetic instruments. The constitutive equations and dynamics that govern the distribution of these unusual events are not well understood, and the relationships between slow deformation and fast seismic ruptures are obscure. The goal of the research reported here is to assess the utility of space-geodetic data in elucidating infraseismic and subseismic phenomena. Specific objectives of this project include the use of existing seismological, geodetic, and other data to characterize the distribution of infraseismic and subseismic transients and the development of strategies for space-geodetic monitoring of infraseismic and subseismic transients along major plate boundaries. This research contributes to NASA's program in solid-earth dynamics by helping to elucidate the temporal and spatial scales for deformation transients that might be observed by space-geodetic methods. It has the potential to yield new insights into the dynamics of large earthquakes, and it may help to elucidate the general issue of earthquake predictability.

In previous years our group has identified slow and quiet earthquakes by measuring low-frequency spectrum of the seismic source using a variety of traveling and standing wave techniques. Substantial progress has been made towards cataloging the occurrences slow earthquakes and slow-precursor earthquakes. This progress is documented in the following publications:

Jordan, T. H., Far-field detection of slow precursors to fast seismic ruptures, *Geophys. Res. Lett.*, **18**, 2019-2022, 1991.

Ihmlé, P.F., P. Harabaglia, and T. H. Jordan, Teleseismic detection of a slow precursor to the great 1989 Macquarie Ridge earthquake, *Science*, **261**, 177-183, 1993.

Ihmlé, P.F., and T. H. Jordan, Teleseismic search for slow precursors to large earthquakes, *Science*, **266**, 1547-1551, 1994.

Ihmlé, P. F., and T. H. Jordan, Source time function of the great 1994 Bolivia deep earthquake by waveform and spectral inversion, *Geophys. Res. Lett.*, **22**, 2253-2256, 1995.

Since January, 1996, we have focused on observing slow precusors to large earthquakes in the time domain. This is an important observational task both for establishing the existence of slow precursors and for characterizing the signals that might be measurable geodetically before the onset of the fast rupture during such an event. The detection of slow precursors as time domain signals at teleseismic distances is difficult because ambient level of seismic noise rises rapidly at frequencies below about 3 mHz. We have detected such signals for the March 14th, 1994 Romanche Transform earthquake ($M_W$ 7.0). On broadband teleseismic records, the event sequence begins with a small ($M_W$ ~6) preshock, followed 16 s later by the mainshock. However, low-pass filtered version of the vertical-component, low-noise

records display precursory ramps with the same polarity as the mainshock P-wave. This feature is most obvious for TAM, the closest low-noise station, where the ramp begins at least 80 s before the preshocks's high-frequency P-wave arrival time. Stations at greater distances have lower signal to noise ratios, but a stack of the six best records yields a ramp with a duration and amplitude similar to the precursor seen at TAM (Figure 1). Network-averaged amplitude and phase-delay spectra in the frequency range 1-50 mHz have been inverted for the source time function (STF) using the procedures of Ihmlé et al. (1993). The amplitude spectra show a break around 8 mHz, below which the amplitude increases sharply, similar to many events reported by Ihmlé et al (1993) and indicative of a compound source. An adequate fit to the spectral data cannot be obtained without moment release prior to the preshock's high-frequency origin time. The best models are characterized by a smooth, precursory ramp with a duration of 80-100 s, followed by a moment rate peak associated with the preshock and a much larger mainshock peak. The spectral data are thus consistent with the time domain observations. We invert both the time-domain stack and network-averaged spectra to obtain an STF (figure 2). We find that the precursory ramp is part of a slow event whose total moment is 35% of the mainshock moment.

The Romanche transform is also an ideal plate boundary for studying the accommodation of seismic deficit by slow slip. Five events with moments greater than $1 \times 10^{26}$ dyne-cm have occurred on the Romanche transform fault since 1980. The low-frequency spectra of all five events show the type of slope break we interpret as resulting from a compound event. In each case, the slow portion of the event accounts for 30-50% of the total moment released by the earthquake. Hence, on this transform, some significant portion of the total slip is accommodated by slow smooth faulting.

The paper on the Romanche event's slow precursor is in press in *Science* (attached).

McGuire, J. J., Ihmlé, P. F., and Jordan, T. H., Time-Domain Observations of a Slow Precursor to the 1994 Romanche Transform Earthquake, *Science* (in press) 1996.

We have also presented the work on the 1994 Romanche event at the 1996 IRIS workshop, and we have submitted an abstract on the Romanche event for the 1996 fall AGU meeting. The Romanche event points out the difficulty of observing slow precursors in the time-domain. Despite the large total moment of the event, the precursory signals are barely above the noise level. We are conducting a survey of all events from 1995 to present to identify other slow precursor events in the time domain using nearby low-noise stations.

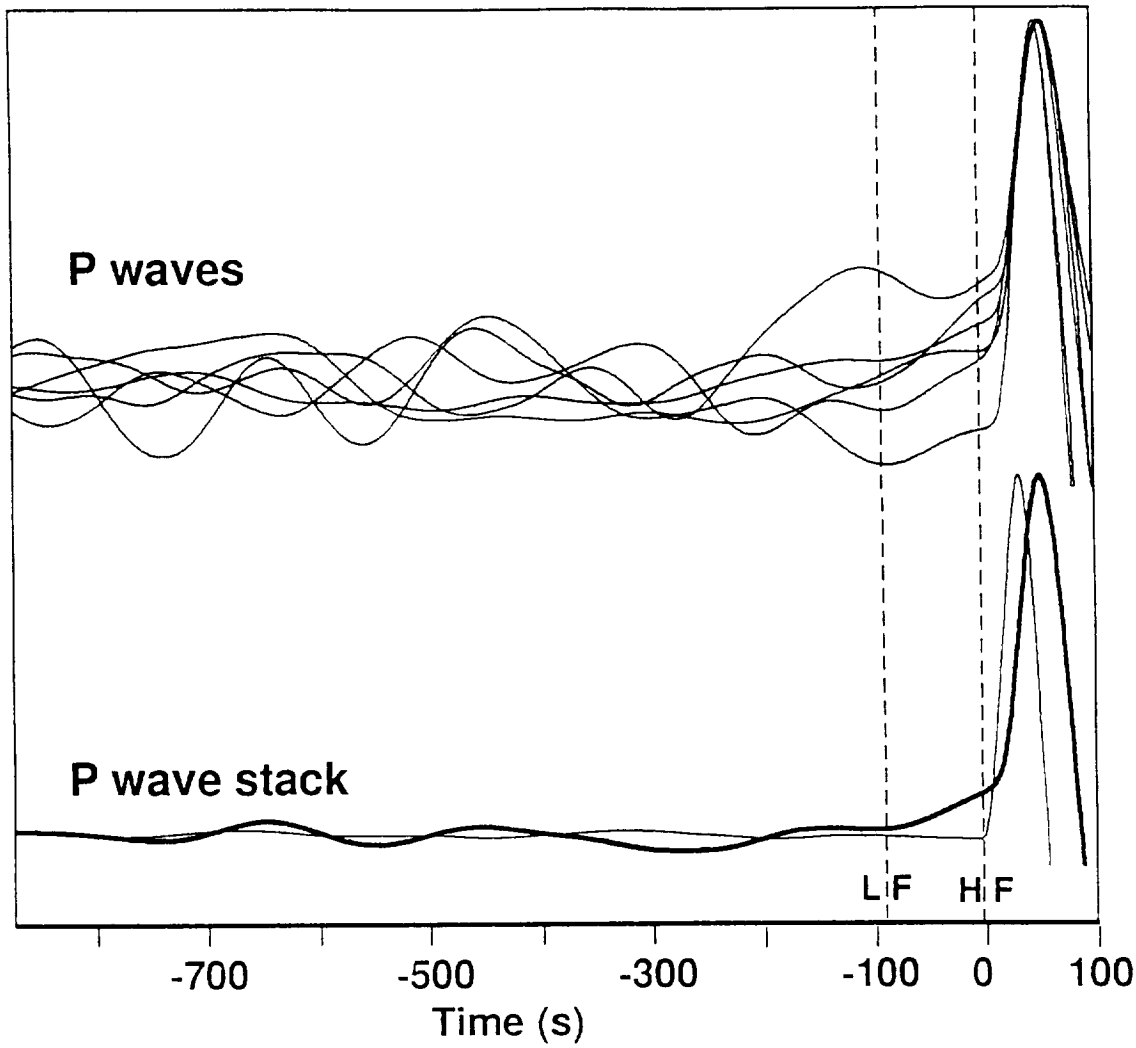


Fig 1. Upper traces are vertical-component P waves for the 1994 Romanche Transform earthquake for the six lowest noise stations. These were the only stations for which the first swing of the main shock P wave was greater than a factor of three above the noise level. All seismograms have been detided, low-pass filtered (4-pole Butterworth with a corner at 6 mHz), corrected for the group delay of the filter, detrended, and corrected for the radiation pattern (flipped polarity if dilitational and normalized to a common amplitude). Lower traces are a stack of these six seismograms (heavy line) and a similar, six station stack for the large (M 7.0) Mendocino earthquake of 1 September 1994 (light line). In both cases, zero time corresponds to the high frequency arrival time (labelled HF). The Romanche Transform earthquake shows a precursory ramp beginning at or before -90 s (labelled LF), whereas the Mendocino earthquake does not. The delay in the arrival time of the high-amplitude P wave for the Romanche Transform earthquake corresponds approximately to the 16-2 delay between the high frequency origin time and the onset of the main pulse of moment release.

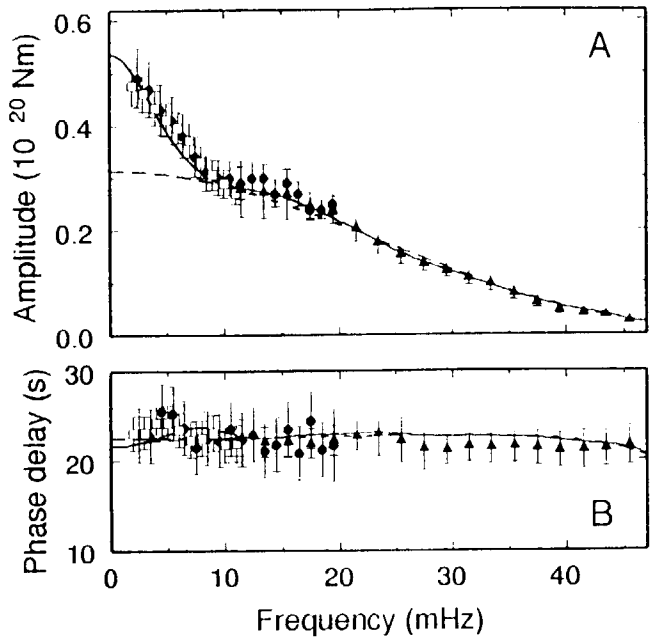


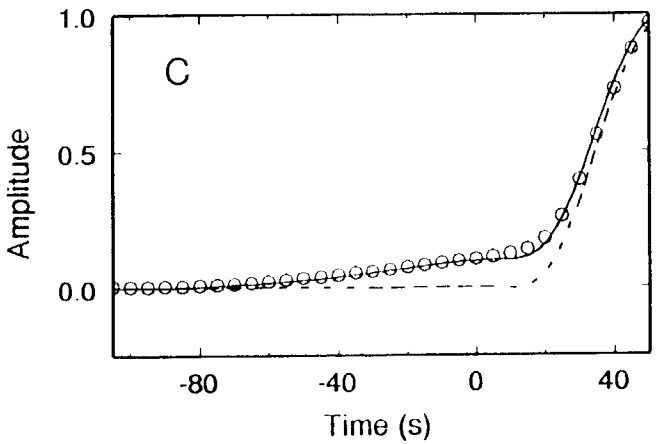


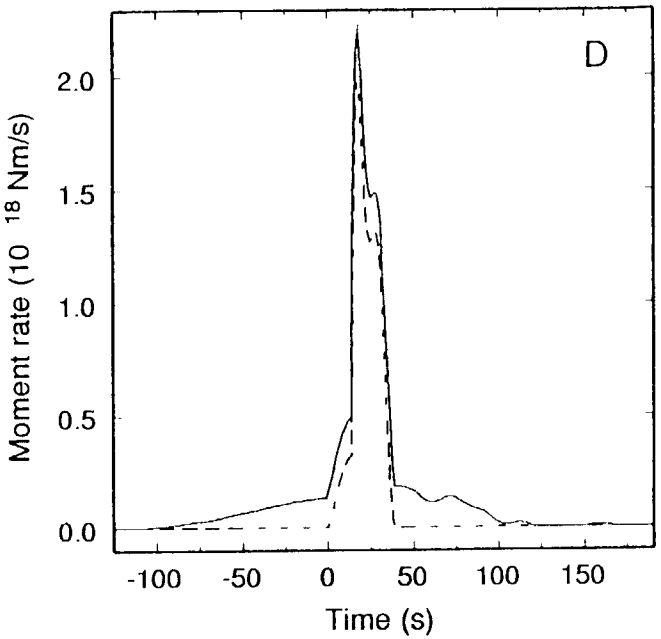


Fig 2. (A) Amplitude and (B) phase-delay spectra for the 1994 Romanche Transform earthquake. Points are estimates with one sigma error bars obtained from propagation corrected spectra, averaged over a global network of 32 broadband stations; wave types used in the measurements are spheroidal free oscillations (solid circles), Rayleigh waves (open squares) and long-period body wavetrains (triangles). Solid and dashed lines are the spectra obtained by Fourier transforming the source time functins in D. The phase delay spectrum is referenced to the NEIC high-frequncy origin time. (C) Comparision of the observed P-wave stack from Fig. 1. (open circles) with synthetic seismograms (solid and dashed lines) computed from the source time functions in panel (D). (D) The solid line is the source time function obtained by joint inversion of the spectral-domain data in (A) and (B) and time domain data in (C). The dashed line is from the inversion of just the spectral data in the band from 10-50 mHz, where the time function was restricted to be zero for time less than 0 x and greater than 45 s.

# Time-Domain Observations of a Slow Precursor to the 1994 Romanche Transform Earthquake

Jeffrey J. McGuire*, Pierre F. Ihmlé, Thomas H. Jordan

Low-frequency spectral anomalies have indicated that some large earthquakes are preceded by extended episodes of smooth moment release, but the reality of these slow precursors has been debated because they have not been directly observed in the time domain. High-gain seismograms from the 14 March 1994 Romanche Transform event ($M_W$ 7.0) show a precursory ramp with a moment of 7 x $10^{18}$ Newton-meters beginning about 100 seconds before the arrival of the high-frequency *P* waves. This precursor was the initial phase of a slow component of slip that released nearly half of the total moment of the earthquake. Such behavior may be typical for large earthquakes on the oceanic ridge-transform system.

Since the early work of Kanamori and Cipar (*1*) on the great 1960 Chilean earthquake, episodes of slow, smooth moment release have been postulated to precede and initiate some large earthquakes. New techniques have recently been developed for the detection and analysis of slow precursors using low-frequency seismic spectra (*2,3*). Their application to a catalog of large events has revealed that slow precursors are rare in continents and convergence zones but appear to be common features of earthquakes on the oceanic ridge-transform system (*4*). For example, Ihmlé *et al.* (*3*) found that the great Macquarie Ridge earthquake of 23 May 1989, which had a

Jeffrey J. McGuire and Thomas H. Jordan, Department of Earth, Atmospheric and Planetary Sciences, Massachusetts Institute of Technology, Cambridge, MA 02139, USA.

Pierre F. Ihmlé, Institut de Physique du Globe, 4 Place Jussieu, Paris Cedex 75252, France.

* To whom correspondence should be addressed.

moment-magnitude ($M_W$) of 8.2, was preceded by a slow precursor with a moment release of about $3 \times 10^{20}$ Newton-meters (N-m), equivalent to a $M_W$ 7.6 event. However, no precursor was evident on high-gain, broadband seismograms in the interval immediately before the high-frequency *P*-wave arrival times (*3*). This observation has led some to reject the slow-precursor hypothesis (*5*).

The detection of slow precursors as time-domain signals at teleseismic distances is difficult because the ambient level of seismic noise rises rapidly at frequencies below about 3 millihertz (mHz) (*6*). Here we report the detection of such signals for the 14 March 1994 earthquake on the Romanche transform fault in the central Atlantic ocean (Fig. 1). This large earthquake ($M_W$ 7.0) comprised at least two ordinary ruptures, a small preshock (event A in Fig. 2) followed approximately 16 s later by the mainshock (event B). At the lowest noise station, Tamanrasset, Algeria (TAM), a low-passed version of the *P* wave shows a distinct ramp in front of the mainshock (Fig. 2). The amplitude of the ramp exceeded the noise level for at least 100 s before the high-frequency (A) arrival time, and there is some suggestion that its beginning may have preceded A by as much as 300 s.

Although TAM shows the precursor most clearly, the signal is visible at all other stations where the first swing of the low-passed, mainshock *P* wave was greater than a factor of three above the noise level (Fig. 3). On each of the six records that satisfy this criterion, the mainshock *P* wave was preceded by a ramp of the same polarity, and in all six the ramp has a consistent relative slope and duration. Because the low-noise stations cover all four quadrants of the focal sphere and sample epicentral distances ranging from 28° to 73°, these observations confirm that the ramp is a source signal with a radiation pattern similar to the mainshock rather than a propagation effect. Given the coherency of the six low-passed records, we stacked them to obtain a composite waveform (lower part of Fig. 3). When corrected for the group delay of the low-pass filter, the precursory ramp can be seen at least 90 s before the event-A arrival time. As illustrated in Fig. 3, a similar stack of another strike-slip earthquake yielded no such precursor.

The A and B subevents have an unusual space-time relationship that also suggests precursory moment release. We picked the *P*-wave times of the two subevents on all records with clear arrivals (Fig. 4) (*9*), located them relative to the background seismicity (*10*), and aligned the seismicity with the Africa-South America plate boundary on a high-resolution map of the altimetric gravity field (Fig. 5). We found that the two subevents were separated by 83 ± 15 km and 16.7 ± 1.0 s. Therefore, a model of the rupture initiating at A and propagating directly to B requires a rupture velocity of 5.0 ± 1.0 km/s, which exceeds the shear-wave speed in the upper oceanic lithosphere and thus the typical rupture velocity of shallow-focus earthquakes (*13*). Moreover, the A and B locations lie along an azimuth of N37 ± 8°E, which is at a significant angle to the strikes of the inferred fault planes for both subevents (Fig. 5). These data suggest that the two events occurred on separate fault planes and were initiated by a common precursor.

The location of event A, the small preshock ($M_W \sim 6$), is consistent with it being on the primary active trace of the Romanche transform fault, but event B, the mainshock, is located significantly north of this feature, in a valley with a trend nearly parallel to the transform fault (*15*). The directivity inferred from the azimuthal variation of the *P* waveforms indicates that the mainshock propagated to the east. No aftershocks were teleseismically recorded, so we could not determine its rupture length, but standard scaling relations would imply that it was 50 to 70 km (*14*). This approximates the length of a seismic gap just south of the mainshock, where the valley of the main fault trace is interupted by a large bathymetric high (*15*).

It is not possible to locate the slow precursor relative to the mainshock, but moment-tensor inversions exclude the possibility that the precursor occurred on a fault connecting the A and B events (*12*). One scenario consistent with the available data (among many) is that smooth slip at depth in the normally aseismic region redistributed stress in the region and triggered seismicity in both the westernmost portion of the Romanche (A event) and the neighboring fault valley to the north of the seismic gap (B event).

We also investigated the 1994 Romanche Transform earthquake using the spectral synthesis and inversion methods applied in previous studies of slow earthquakes (*2-4*). We estimated the

amplitude (total-moment) spectrum $M_T(\omega)$ and phase delay (time-shift) spectrum $\Delta t(\omega)$ of the source at 1-mHz intervals from 1 to 50 mHz using a combination of body waves, surface waves, and free oscillations (Fig. 6). The different wave types yielded consistent results throughout their regions of overlap. The phase-delay spectrum is nearly constant across the entire frequency band, but the amplitude spectrum shows a sharp break at about 10 mHz. This pattern is similar to that observed for other slow earthquakes by Jordan (2) and Ihmlé and Jordan (4), which they interpreted as compound sources. According to this hypothesis, the amplitude break results from the superposition of an ordinary fast rupture, which dominates the spectrum at high frequencies, and a smooth transient of longer duration, which dominates at low frequencies. The lack of a corresponding break in the phase-delay spectrum requires that the centroid times of the two events are nearly equal, thus impling that the slower event begins first.

To quantify these statements, we performed a joint inversion of the spectra and the *P*-wave stack for the source time function (Fig. 6). The results show an event sequence that comprises a slow earthquake beginning 110 s before the high-frequency origin time ($t = 0$) and continuing for about 250 s, a preshock initiating at 0 s, and a 29-s pulse of high moment release beginning at 16 s. This compound-event model fits the amplitude and phase-delay data across the entire frequency range, as well as the precursor observed in the waveform stack. We also inverted the spectral data alone, allowing no moment release at $t < 0$, but found that we could not simultaneously satisfy the large amplitudes and flat phase-delays at low frequencies. Hence, the spectral data confirm the existence of the slow precursor seen in the *P*-wave stack.

The best-fitting source time function has a total static (zero-frequency) moment of $5.4 \times 10^{19}$ N-m. Comparing its amplitude spectrum to one from a source time function confined to the interval $0 \le t \le 40$ s (Fig. 6) indicates that the static moment released by the slow component is about $2.3 \times 10^{19}$ Nm, or 43% of the total. About $0.7 \times 10^{19}$ Nm (13%) is released in the slow precursor.

Since slow earthquakes occur most frequently along oceanic transform faults, Ihmlé and Jordan (4) proposed that the intrinsic stratification of oceanic lithosphere may be responsible for

their compound-event character. According to this hypothesis, fast ruptures in the shallow seismogenic zone are initiated by the loading due to slower episodes of slip in the subjacent, serpentinized upper mantle. The superposition of a fast event in the middle of a slow event, as seen in the source time function of Fig. 6, is most easily explained by this depth relationship.

The data presented here indicate that the slow precursor of the Romanche earthquake grew for at least 100 s before it triggered a fast rupture, and the total moment released during the entire slow event was comparable to that of the mainshock. This behavior appears to be common on oceanic transform faults (*4*), but it is in marked constrast to the nucleation phases observed for other earthquakes, which are small and accelerate quickly into inertia-dominated instabilities (*18*). The shape of the waveform stack and the absence of any observable high-frequency energy prior to event A indicate that the precursor's moment rate increased smoothly at a nearly linear rate, which implies that the product of the rupture and particle velocities during slow phase of slippage must be at least two orders of magnitude smaller than that during the mainshock (*19*). Hence, the designation "slow precursor" is truly warranted.

## REFERENCES AND NOTES


1. H. Kanamori and J. Cipar, *Phys. Earth Planet. Inter.* **9**, 128 (1974); see also I. L. Cifuentes and P. G. Silver, *J. Geophys. Res.* **94**, 643 (1989).
2. T. H. Jordan, *Geophys. Res. Lett.* **18**, 2019 (1991).
3. P. F. Ihmlé, P. Harabaglia, T. H. Jordan, *Science* **261**, 177 (1993).
4. P. F. Ihmlé and T. H. Jordan, *Science* **266**, 1547 (1994).
5. S. Kedar, S. Watada, and T. Tanimoto, *J. Geophys. Res.* **99**, 17893 (1994), found significant amplitude and phase anomalies for certain low-frequency spheroidal modes that could be explained by a slow precursor to the Macquarie Ridge earthquake [see also J. Park, *Geophys. Res. Lett.* **17**, 1005 (1990)], but they rejected this possibility because no precursor was evident as time-domain signals preceding the *P* waves at high-gain seismic stations. Such

signals would be below the noise level if the time function of the precursor were smooth and of sufficiently long duration (3).

6. D. Agnew and J. Berger, *J. Geophys. Res.* **83**, 5420 (1978); G. C. Beroza and T. H. Jordan, *ibid.* **95**, 2485 (1990).

7. The hypocenter location given by the National Earthquake Information Center is 94:03:14:04:30:07.7 UT, 1.08°S, 23.9°W, h = 10 km, and the Harvard centroid location [A. M. Dziewonski, G. Ekström, M. P. Salganik, *Phys. Earth. Planet. Inter.* **86**, 253 (1994)] is 94:03:14:04:30:33.1 UT, 0.88°S, 23.0°W, h = 15 km.

8. The Harvard centroid location [A. M. Dziewonski, G. Ekström, M. P. Salganik, *Phys. Earth. Planet. Inter.* **90**, 1 (1995)] for this right lateral $M_W$ 7.0 event is 94:09:01:15:16:00.6 UT, 40.59° N, 125.78° W, h = 15km.

9. We picked 10 arrivals for event A and 11 for event B, obtaining at least two B-A differential travel times in each azimuthal quadrant. These differential times are listed with the station azimuths and epicentral distances in the following table:

| Station | Azimuth (deg) | Distance (deg) | B-A Time (s) |
|---|---|---|---|
| ECH | 25 | 56 | 12.4 |
| SSB | 25 | 53 | 11.3 |
| TAM | 48 | 37 | 10.8 |
| LBTB | 121 | 53 | 18.4 |
| BOSA | 125 | 54 | 14.5 |
| BDFB | 238 | 28 | 21.7 |
| LPAZ | 249 | 46 | 24.1 |
| SJG | 297 | 46 | 18.8 |
| ANMO | 305 | 85 | 14.5 |
| CCM | 310 | 73 | 16.8 |

10. Relocations were performed using the clustered-event algorithm of T. H. Jordan and K. A. Sverdrup, *Bull. Seismol. Soc. Am.* **71**, 1105 (1981), which yields relative locations that are

independent of common path anomalies. We relocated the A and B subevents together with all events having 30 or more *P*-wave arrival times in the ISC catalog from 1964-1987 and in the PDE catalog from 1990-1995. All event depths were fixed at 10 km. The hypocentroid of this seismicity cluster has been shifted 12 km in the direction N30°E to align the seismicity with the plate boundaries observed in the gravity field. Although the arrival time data for the two-year period 1988-1989 were unavailable, the PDE catalog shows no events in the aseismic region between 22.3°W and 23.3°W.

11. D. Sandwell, *Eos* **76**, 149 (1995).

12. The moment tensor was determined in 1-mHz bands from 1 to 11 mHz using the free-oscillation inversion method described in M. A. Riedesel, T. H. Jordan, A. F. Sheehan, and P. G. Silver, *Geophys. Res. Lett.* **13**, 609 (1986); no significant frequency dependence of the source mechanism was observed, implying that the slow component of the 1994 Romanche Transform earthquake had a radiation pattern similar to the mainshock. The mechanism labelled LF in Fig. 5 is the average across the frequency band 3-6 mHz. The source mechanisms of the A and B subevents, also shown in Fig. 5, were determined by waveform analysis. They are similar, but not identical; for example, their long-period *P*-wave polarities are reversed at Naña, Peru (NNA).

13. While rupture velocities of shallow-focus earthquakes have been known to exceed the local shear-wave speed [R. Archuleta, *J. Geophys. Res.* **89**, 4559 (1984)], they are rare. Typical rupture velocities of shallow-focus earthquakes are less than 3.5 km/s (*14*).

14. C. H. Scholz, *The Mechanics of Earthquake Faulting*, Cambridge University Press, Cambridge, 1990, 439 pp.

15. E. Bonatti, M. Ligi, L. Gasperini, A Peyve, Y. Raznitsin, Y. J. Chen, *J. Geophys. Res.* **99**, 21779 (1994); R. C. Searle, M. V. Thomas, E. J. W. Jones, *Mar. Geophys. Res.* **16**, 427 (1994). The morphology of the western portion of the Romanche Transform is extremely complex, exhibiting multiple paleotransform valleys that resulted from past changes in plate motions. The seismic gap on the main transform trace between 22.3°W and 23.3°W (Fig. 4)

corresponds to a bathymetric high, which Searle *et al.* attribute to transpression caused by the northeastward bending of the fault trace at the western end of the gap. Locking of the main trace in this region could explain the offset of the event-B rupture to the north.

16. The spectral estimates in Fig. 6 were obtained using the procedures described in (2-4). Measurements of spheroidal free oscillations were made from vertical-component seismograms in the 1-19 mHz band using the methods of P. G. Silver and T. H. Jordan, *Geophys. J. R. Astron. Soc.* **70**, 755 (1982), and M. A. Riedesel and T. H. Jordan, *Bull. Seismol. Soc. Am.* **79**, 85 (1989). Measurements of first-orbit Rayleigh waves (1-10 mHz) and long-period body wavetrains (10-50 mHz) were obtained from vertical-component seismograms by the methods of Ihmlé *et al.* (3). In all cases, synthetic seismograms were used to account for radiation-pattern and propagation effects. The synthetics were computed by mode summation from the Harvard CMT (7) and the degree-12 aspherical earth structure of W.-J., Su, R. L. Woodward, and A. M. Dziewonski, *J. Geophys. Res.* **99**, 6945, (1994). Fundamental modes above 7 mHz were also corrected for smaller-scale heterogeneity using the degree-36 phase-velocity maps of G. Ekström, J. Tromp, and E. W. Larson, *Eos* **74**, 438 (1993).

17. The data were inverted using the quadratic programming algorithm of Ihmlé *et al.* (3), which minimizes a linear combination of a chi-square measure of data misfit and a quadratic form measuring the smoothness of the source time function, subject to the constraint that the source time function be nonnegative. The smoothing varied from high values prior to the event-A origin time ($-10 \le t < 0$ s), which insured that the precursor did not generate significant high-frequency arrivals, to low values during the mainshock phase of the rupture ($16 \le t < 45$ s), when the high-frequency amplitudes were largest; intermediate values of smoothing were assumed between the initiation of event A and the initiation of event B ($0 \le t < 16$ s) and in the interval after the mainshock ($40 \le t < 200$ s).

18. W. L. Ellsworth and G. C. Beroza, *Science* **268**, 851 (1995), have shown that the nucleation phases for typical earthquakes release about 0.5% of the total static moment $M_0$ and that the

duration of nucleation varies as $M_0^{1/3}$. These scaling relationship yield a nucleation phase with a moment of about $1.5 \times 10^{17}$ Nm and a duration of about 2 s for an earthquake the size of the 1994 Romanche Transform mainshock.

19. For a rectangular fault of depth $D$ slipping at a constant particle velocity $\Delta\dot{u}$ and growing unilaterally at a rupture velocity $v_r$, the moment rate will increase at a rate $\dot{M} = 2\mu D v_r \Delta\dot{u}$, where $\mu$ is the shear modulus. The observed moment acceleration for the slow precursor of the Romanche Transform earthquake is about $1.8 \times 10^{17}$ Nm/s$^2$. For $D$ = 10 km and $\mu$ = $3 \times 10^{10}$ Pa, we obtain $v_r \Delta\dot{u} \approx 3$ m$^2$/s$^2$. Hence, if $v_r \approx 100$ m/s, $\Delta\dot{u} \approx 0.03$ m/s. In contrast, the observations for ordinary earthquakes, including the mainshock of this event (Fig. 5), yield $v_r \Delta\dot{u} > 1000$ m$^2$/s$^2$.

20. We thank H. Webb for assistance with the gravity data and G. Ekström, J. Tromp, and E. Larson for the use of their unpublished phase-velocity maps. We are grateful to Doug Wiens and an anonymous reviewer for helpful comments that improved the manuscript. This research was sponsored by the U.S. National Science Foundation under grant EAR-9305081 and the National Aeronautics and Space Administration under grant NAG5-1905. P. F. I. was partially supported by the Swiss National Science Foundation.

## Figure Captions

Fig. 1. Map showing the Harvard Centroid Moment Tensor (CMT) location and mechanism of the 14 March 1994 Romanche Transform earthquake (7). Triangles are the locations of the six seismic stations used in the *P*-wave stack; these stations sample all four quadrants and lie away from nodes in the radiation pattern.

Fig. 2. Vertical-component records of the *P* wave from the 1994 Romanche Transform earthquake at the high-performance seismic station TAM. Top panel contains the raw broadband trace at two magnifications (both labeled BHZ) and a detided, low-pass filtered version of the same seismogram (labeled LOW), revealing the precursory ramp beginning at least 1 min before the high-frequency arrival time ($t = 0$). The low-pass filter is a 4-pole Butterworth with a 6-mHz corner. Vertical scales are digital units of the seismogram (counts). Arrows are the arrival-time picks for subevents A and B, with zero time set to be the high-frequency (event-A) arrival time. A comparison of the lower two traces, which have the same magnification, shows that the amplitude of the high-frequency noise is substantially larger than that of the low-frequency precursor, masking the latter on the unfiltered record. The lower panel is the same low-passed record at a longer time scale, with dashed lines approximating noise level. The two low-passed records have not been corrected for the group delay of the filter, which is 10 s.

Fig. 3. Upper traces are vertical-component *P* waves for the 1994 Romanche Transform earthquake for the six, low-noise stations shown in Fig. 1. These were the only stations where the first swing of the main shock *P* wave was greater than a factor of three above the noise level. All seismograms have been detided, low-pass filtered (4-pole Butterworth with a corner at 6 mHz), corrected for the group delay of the filter, detrended, and corrected for radiation pattern (flipped in polarity if dilatational and normalized to a common amplitude). Lower traces are a stack of these six seismograms (heavy line) and a similar, six-station stack for the large ($M_W$ 7.0) Mendocino earthquake of 01 September 1994 (*8*) (light line). In both cases, zero time corresponds to the high-frequency arrival time (labelled HF). The Romanche Transform earthquake shows a precursory ramp beginning at or before −90 s (labelled LF), whereas the Mendocino earthquake does not. The delay in the arrival time of the high-amplitude *P* wave for the Romanche

Transform earthquake corresponds approximately to the 16-s delay between event A, which is the first high-frequency arrival, and event B, which is the mainshock.

**Fig. 4.** Vertical-component, *P* waves recorded at four stations, showing the arrival-time picks for event A on high-pass filtered seismograms (lower traces) and event B on unfiltered, broadband seismograms (upper traces). Each trace runs from 20 s before to 30 s after the event-A arrival. The high-pass filter is a 4-pole Butterworth with a 1-Hz corner. $\phi$ is the station azimuth. Stations to the northeast (e.g., TAM) have smaller B-A time differences than stations to the southwest (e.g., LPAZ), indicating that event B is northeast of event A (*9*).

**Fig 5.** Map of the western part of the Romanche transform fault, showing the relocated earthquakes, plotted as points with 95% confidence ellipses (*10*), and the altimetric gravity field, plotted in color (*11*). Beachball insets are the low-frequency source mechanism (LF) and subevent mechanisms (A and B) for the 1994 Romanche Transform earthquake (*12*). Large dots are the epicenters of the A and B subevents and the Harvard CMT epicentroid, and the arrow emanating from B shows the direction and approximate length of the main rupture. The gravity anomalies range from –15 milligals (blue) to +15 milligals (red), and the relief is illuminated from the northwest.

**Fig. 6.** (**A**) Amplitude and (**B**) phase-delay spectra for the 1994 Romanche Transform earthquake. Points are estimates with one-sigma error bars obtained from propagation-corrected spectra, averaged over a global network of 32 broadband stations (*16*); wave types used in the measurements are spheroidal free oscillations (solid circles), Rayleigh waves (open squares), and long-period body wavetrains (solid triangles). Solid and dashed lines are the spectra obtained by Fourier transforming the source time functions in panel D. The phase-delay spectrum is referenced to the NEIC high-frequency origin time (*7*), which corresponds to the initiation of event A. (**C**) Comparison of the observed *P*-wave stack from Fig. 3 (open circles) with synthetic seismograms (solid and dashed lines) computed from the source time functions in panel D. (**D**) Solid line is the source time function obtained by the joint inversion of the spectral-domain data in panels A and B and time-domain data in panel C (*17*). Dashed line is from

the inversion of just the spectral data in the 10-50 mHz band, where the time function was restricted to be zero for time less than 0 s and greater than 45 s.

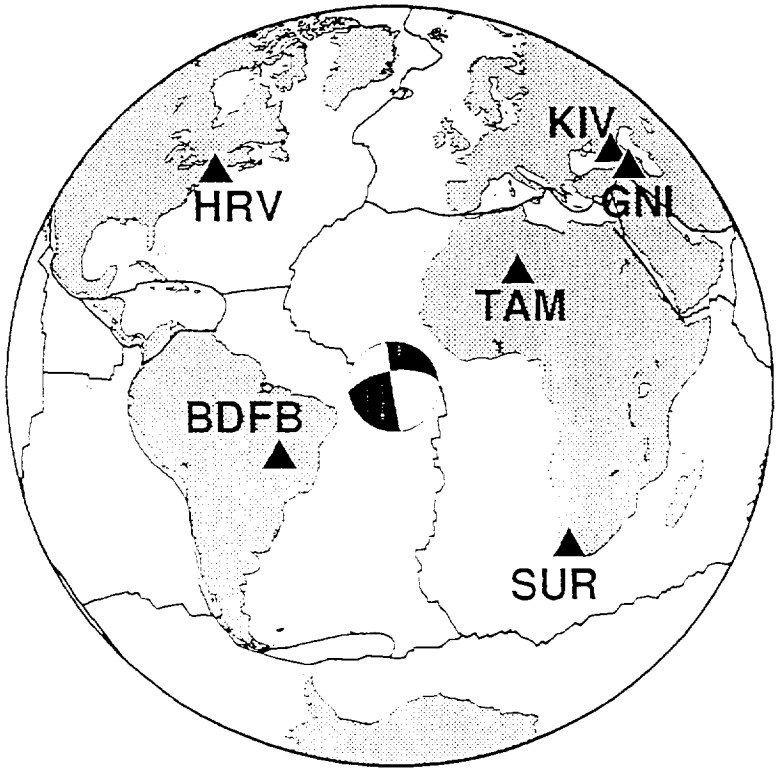


McGuire,Ihmle & Jordan, submitted to Science, June 1996

**Fig. 1**

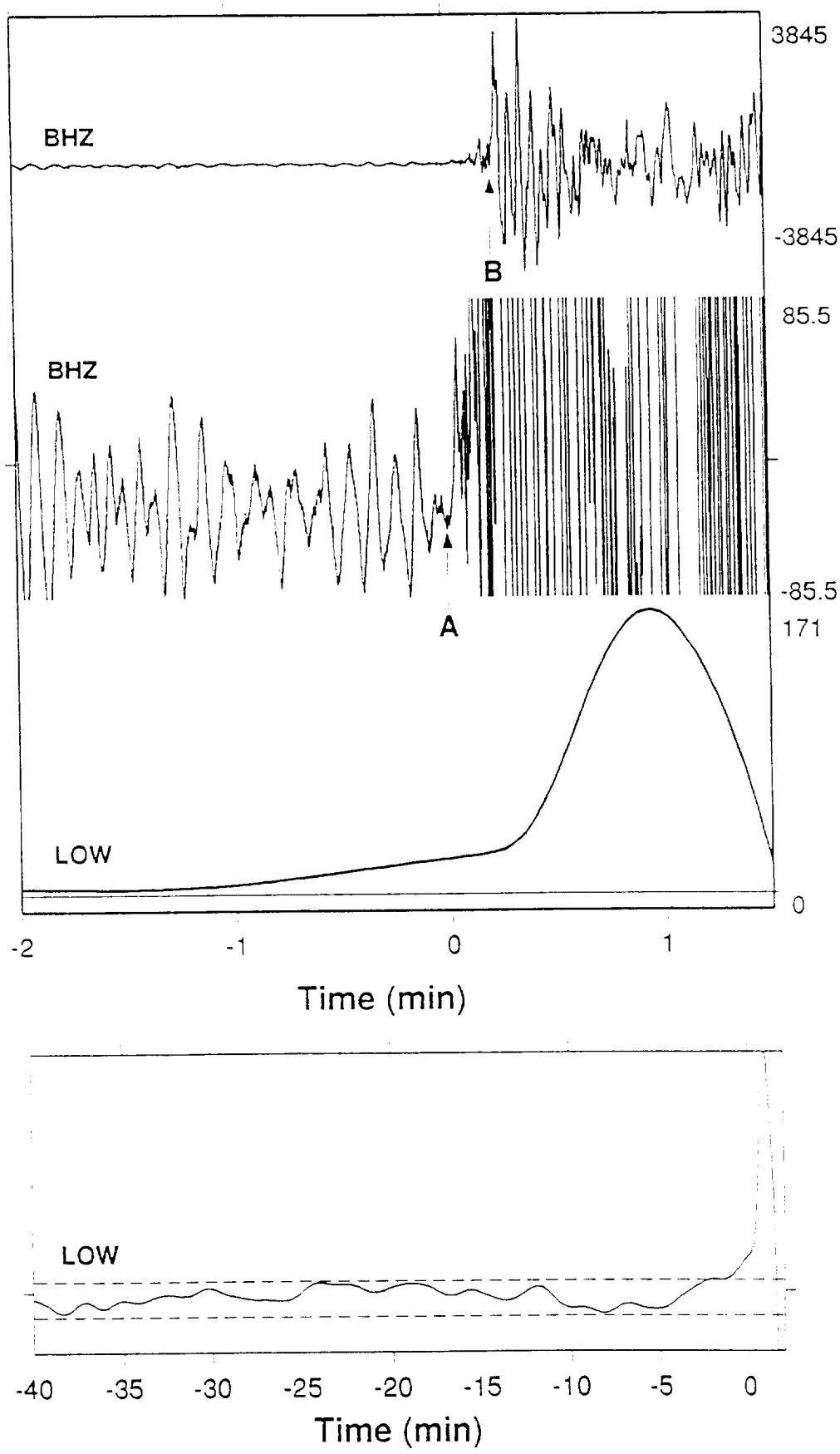


**Figure 2**, McGuire, Ihmle, and Jordan, submitted to Science, June 1996

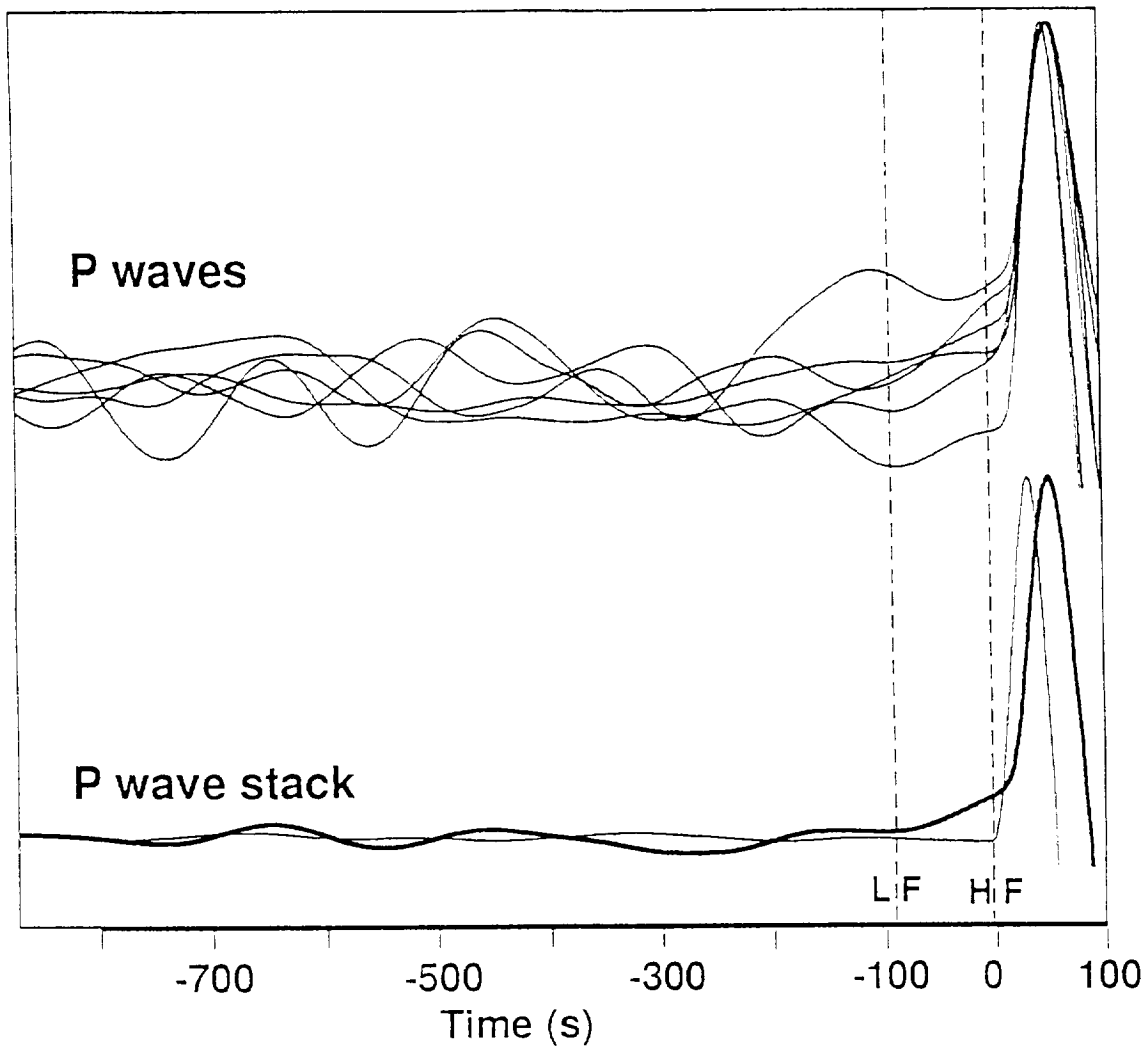


McGuire,Ihmle & Jordan, submitted to Science, June 1996

**Fig. 3**

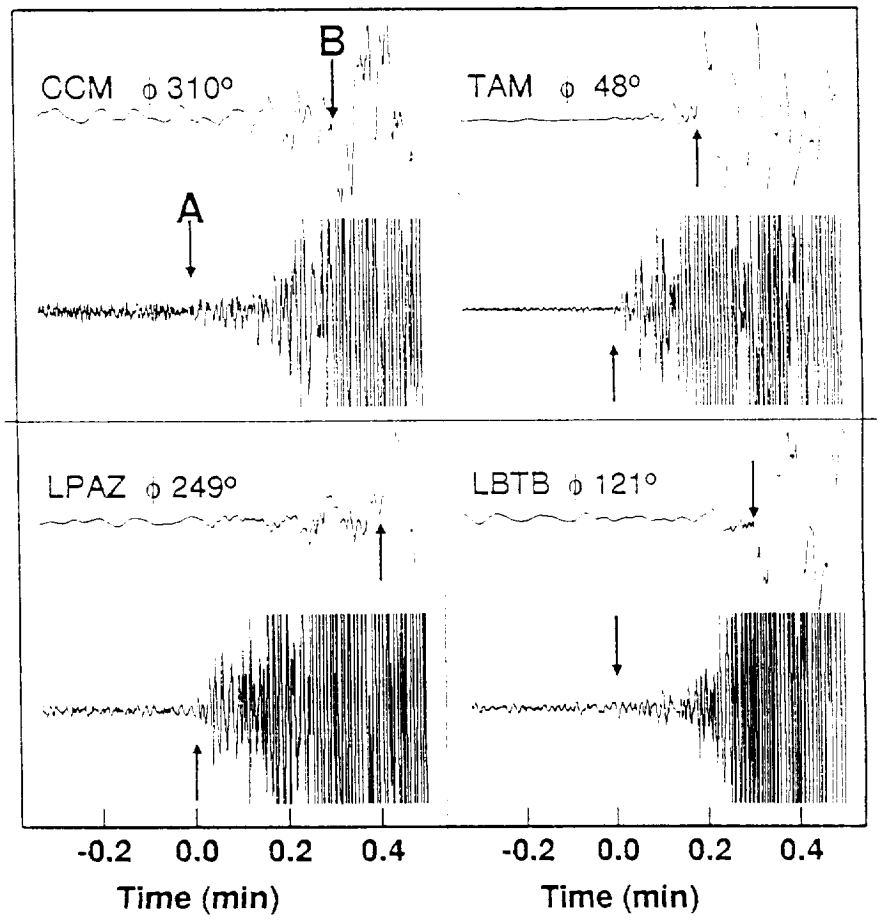


McGuire,Ihmle & Jordan, submitted to Science, June 1996

**Fig. 4**

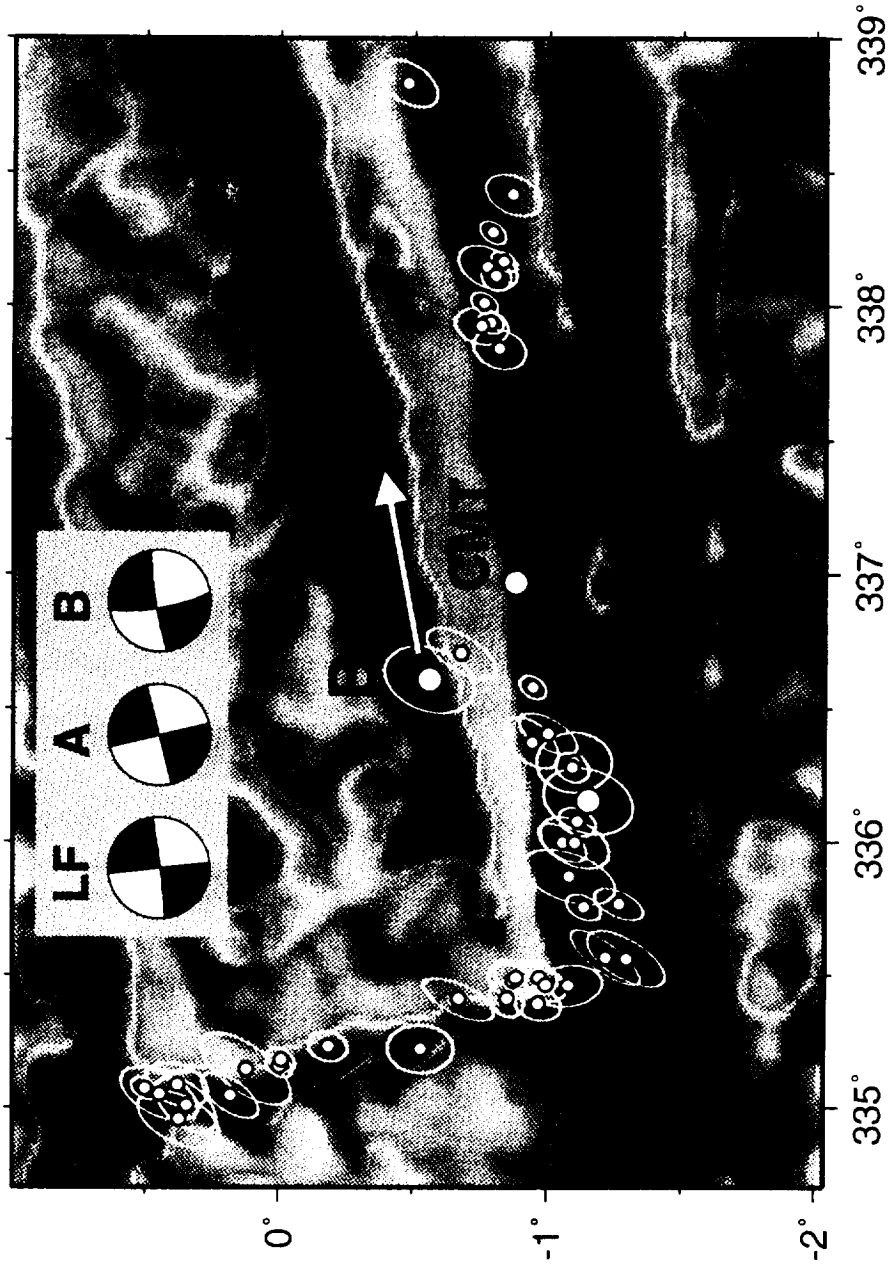


McGuire,Ihmle & Jordan, submitted to Science, June 1996

**Fig. 5**

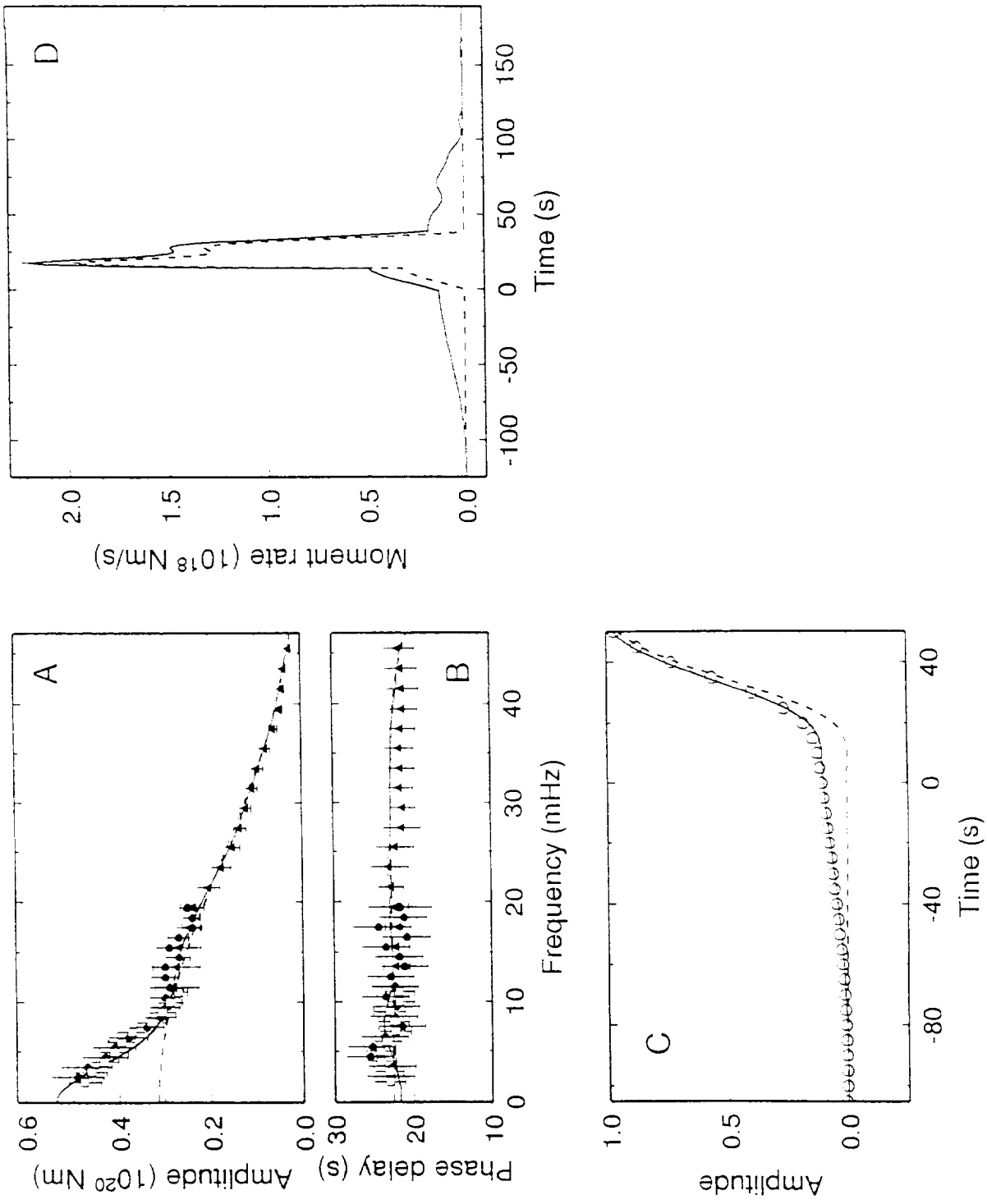


McGuire,Ihmle & Jordan, submitted to Science, June 1996

**Fig. 6**